Regional requirements for Dishevelled signaling during *Xenopus* gastrulation: separable effects on blastopore closure, mesendoderm internalization and archenteron formation

Andrew J. Ewald[1,*], Sara M. Peyrot[2], J. Michael Tyszka[1], Scott E. Fraser[1] and John B. Wallingford[3,†]

[1]Department of Biology and Biological Imaging Center, California Institute of Technology, Pasadena, CA 91125, USA
[2]Department of Molecular and Cell Biology, University of California, Berkeley, CA 94720, USA
[3]Department of Molecular, Cell and Developmental Biology and Institute for Cellular and Molecular Biology, University of Texas, Austin, TX 78712, USA

*Present address: Department of Anatomy, University of California, San Francisco, CA 94143, USA
†Author for correspondence (e-mail: wallingford@mail.utexas.edu)

Accepted 21 October 2004

Development 131, 6195-6209
Published by The Company of Biologists 2004
doi:10.1242/dev.01542

Summary

During amphibian gastrulation, the embryo is transformed by the combined actions of several different tissues. Paradoxically, many of these morphogenetic processes can occur autonomously in tissue explants, yet the tissues in intact embryos must interact and be coordinated with one another in order to accomplish the major goals of gastrulation: closure of the blastopore to bring the endoderm and mesoderm fully inside the ectoderm, and generation of the archenteron. Here, we present high-resolution 3D digital datasets of frog gastrulae, and morphometrics that allow simultaneous assessment of the progress of convergent extension, blastopore closure and archenteron formation in a single embryo. To examine how the diverse morphogenetic engines work together to accomplish gastrulation, we combined these tools with time-lapse analysis of gastrulation, and examined both wild-type embryos and embryos in which gastrulation was disrupted by the manipulation of Dishevelled (Xdsh) signaling. Remarkably, although inhibition of Xdsh signaling disrupted both convergent extension and blastopore closure, mesendoderm internalization proceeded very effectively in these embryos. In addition, much of archenteron elongation was found to be independent of Xdsh signaling, especially during the second half of gastrulation. Finally, even in normal embryos, we found a surprising degree of dissociability between the various morphogenetic processes that occur during gastrulation. Together, these data highlight the central role of PCP signaling in governing distinct events of *Xenopus* gastrulation, and suggest that the loose relationship between morphogenetic processes may have facilitated the evolution of the wide variety of gastrulation mechanisms seen in different amphibian species.

Key words: Gastrulation, Dishevelled, Morphogenesis, *Xenopus*

Introduction

Gastrulation is the first major morphogenetic transformation in embryonic development. In the frog, the process of gastrulation must accomplish two major goals: the closure of the blastopore to bring the endoderm and mesoderm fully inside the ectoderm, and the generation of the archenteron. These end goals are accomplished through the concerted action of several different tissues, each of which engage in distinct cell movements and cell shape changes. The different tissues must require intricate coordination to ensure the successful completion of gastrulation. There are two separate challenges to resolve in frog gastrulation: identifying and understanding the cell and molecular events that take place in each of the different tissues (Keller et al., 2003), and discerning the mechanisms that coordinate these varied events between tissues.

Tissue isolation experiments have permitted the individual events to be studied in detail, and have identified the autonomous morphogenetic processes that drive amphibian gastrulation. For example, isolated head mesoderm moves directionally, mimicking its advance across the intact blastocoel roof (Davidson et al., 2002; Nagel et al., 2004; Winklbauer et al., 1992). Isolated vegetal mass (endoderm) undergoes vegetal rotation movements, much like the early motions in the embryo that expand the blastocoel floor and move mesendoderm into contact with the overlying ectoderm (Winklbauer and Schurfeld, 1999). Finally, explanted axial mesoderm engages in convergent extension, narrowing and lengthening to adopt the elongate morphology appropriate for the forming body axis (Holtfreter, 1944; Keller and Danilchik, 1988; Schectman, 1942; Wilson and Keller, 1991). Such explant experiments have been central to our understanding of the cell behaviors driving each of these morphogenetic processes. For example, time-lapse imaging of cells in the *Xenopus* dorsal marginal zone revealed that convergent extension is driven by mediolateral cell intercalation; detailed imaging experiments demonstrated that the intercalation is accomplished by cell protrusions that are stabilized and

polarized mediolaterally (Shih and Keller, 1992a; Shih and Keller, 1992b; Wallingford et al., 2000; Wilson and Keller, 1991). By comparison, much less is understood about the interrelationships between these different autonomous processes, and about their coordination, in the embryo, to accomplish the end goals of gastrulation.

We sought to study the mechanistic connection between different tissue movements during gastrulation in intact embryos. The internal events of gastrulation in *Xenopus* remain poorly understood, largely because of the large size and opaque nature of the early embryo. To better define these internal events, we produced high-resolution 3D digital datasets of fixed frog gastrulae; to examine their coordination in detail, we developed a series of morphometric measurements to simultaneously assess the progress of convergent extension, blastopore closure and archenteron formation in a single embryo. To understand how the diverse morphogenetic engines work together to accomplish gastrulation, we applied these tools to wild-type and experimentally manipulated embryos of various gastrula stages.

Members of the planar cell polarity (PCP) pathway, including Dishevelled, are among the most well-studied genes involved in gastrulation in *Xenopus* (reviewed by Wallingford et al., 2002). In contrast to the patterning defects that result from perturbing the canonical Wnt signaling pathway, the disruption of genes in the Wnt/PCP pathway results in a failure of convergent extension (Darken et al., 2002; Deardorff et al., 1998; Goto and Keller, 2002; Medina et al., 2000; Moon et al., 1993; Park and Moon, 2002; Rothbächer et al., 2000; Sokol, 1996; Takeuchi et al., 2003). Moreover, time-lapse imaging has revealed that cells lacking *Xenopus* Dishevelled (Xdsh) signaling fail to stabilize and polarize the lamellipodia that drive cell intercalation during convergent extension (Wallingford et al., 2000). Disruption of PCP signaling has been shown to result in defective blastopore closure (Sokol, 1996). However, the effect of disrupted Xdsh signaling on other events of gastrulation remains poorly defined.

We show that mesendoderm internalization proceeds very effectively in the nearly complete absence of convergent extension and blastopore closure in embryos with disrupted Xdsh signaling. On the contrary, the failure of blastopore closure in embryos lacking Xdsh was tightly correlated with a failure of convergent extension. In addition, we found that blastopore closure required Xdsh signaling not only in the dorsal marginal zone, but also in the ventral/lateral marginal zone. We also found that archenteron elongation was independent of Xdsh signaling during the second half of gastrulation. In embryos lacking Xdsh function, nearly half of the length of the late gastrula-stage archenteron was generated in the absence of both convergent extension and blastopore closure.

Together, these data highlight the central role of PCP signaling in governing distinct events of *Xenopus* gastrulation, namely convergent extension and blastopore closure. Moreover, the data reveal a surprising degree of dissociability between these processes and mesendoderm internalization and archenteron formation. This loose relationship between morphogenetic processes may have allowed for the evolution of the wide variety of gastrulation mechanisms seen in different amphibian species.

Materials and methods

Embryos, microinjection, and in situ hybridization

Standard procedures were used, as described previously (Sive et al., 2000). Each injected blastomere received 1 ng *Xdd1* mRNA (Sokol, 1996), as well as 0.1 ng *EGFP* mRNA, injected equatorially into two dorsal or ventral blastomeres at the four-cell stage. 'Circumferential' embryos were injected equatorially into all four blastomeres. Embryos were screened for GFP localization before filming or in situ hybridization.

Surface-imaging microscopy

Embryos were fixed in Bouin's fixative and imaged as described (Ewald et al., 2002). Three-dimensional renderings were performed in ResView 3.1 (Resolution Corporation; now Microscience Group, Corte Madera, CA). Images in Fig. 1G-I were processed using Unsharp Mask (75%, radius 5, threshold 0) in Adobe Photoshop 6.0. Surface rendering (Fig. 12) was performed with Amira 3.1 (TGS, San Diego, CA).

Quantification of gastrulation

Intact embryos were photographed externally then bisected with a scalpel and photographed on the cut surface with a Zeiss Axiocam on a Zeiss Axiovert S-100 (Carl Zeiss, Thornwood, NY). Measurements were calculated using custom software developed in MatLab R13 (The Mathworks). Calculations were performed on unprocessed images.

Embryonic center and radius estimates

Assuming that the embryo is essentially spherical allows a geometrically consistent estimate of surface areas from their 2D projection in plane-field micrographs. The embryonic sphere radius and center can be estimated from a circle approximation to the embryo boundary in the 2D image. The center (x_0,y_0) and radius (a) of the circle approximation were calculated from three manually-defined points on the embryo boundary in the plane-field image. Applying the spherical embryo approximation, the elevation (z) of any point (x,y) within the embryo boundary can be estimated using:

$$z = \sqrt{a^2 - [(x-x_0)^2 + (y-y_0)^2]},$$

where the sphere center lies in the plane z=0.

Natural spline tracing of blastopore boundary and surface area ratio calculations

Blastopore and *Xnot* domain boundaries were defined by fitting a closed natural spline to a set of manually selected points in the 2D image. Typically between 5 and 15 points were used to define the spline that was then approximated by a polygon with more than 100 vertices. The true surface area enclosed by the natural spline boundary was calculated by re-projection of the 2D polygon spline approximation to the 3D embryonic sphere surface. The area enclosed by this spherical polygon was determined using a discrete line-integral approach implemented by MatLab. The ratio of the blastopore surface area to the surface area of the embryonic hemisphere was calculated using the radius estimate, a.

Xnot length/width calculations

The length and width of the Xnot domain (von Dassow et al., 1993) were determined by re-projection of the polygon spline approximation to the surface of the embryonic sphere, rotation of the long axis of the domain to the equator followed by determination of the maximum azimuth and elevation extents of the domain. The long axis of the domain was defined as the great circle on the embryo surface passing through the re-projection of two points manually defined in the 2D image. Calculations presented divide the maximum length of the domain by the median width. Ratios calculating median,

maximum and mean width were compared. and gave the same statistical results.

Archenteron and mesendoderm progress calculations

Images of mid-sagittally cleaved embryos were analyzed by manually defining a boundary circle for the embryo as described above. Lines were then defined from the center of the boundary circle to each of four points: the dorsal lip of the blastopore (DBPL), the anterior limit of the Xnot domain, the anterior limit of the archenteron, and the anterior limit of the mesendoderm. All angle differences were calculated between the dorsal lip of the blastopore (Fig. 2D), except for the progress of mesendoderm migration, which was calculated as the angle from the vegetal pole to the leading edge of the mesendoderm. Archenteron extension was calculated as the angle from the DBPL to the anterior limit of the archenteron. Anterior archenteron expansion was defined as the length of the archenteron, in degrees, from the anterior limit of the Xnot domain to the anterior limit of the archenteron. Archenteron inflation was quantified by manually defining the outline of the embryo and of the archenteron (using natural splines) on mid-sagittal surface. Progress in inflation was calculated as the ratio of the area of the archenteron to the area of the embryo.

Time-lapse photography

Embryos were placed vegetal side up in modeling clay-coated dishes, and cultured in 1/3×MMR. Images were collected every 2 minutes on a Leica MZFl III dissecting microscope (Leica Microsystems, Bannockburn, Il), using a Nikon D1x digital camera and Nikon Capture 3 software (Nikon, Melville, CA), running on an iMac (Apple Computers, Cupertino, CA). Time-lapse stacks were assembled in NIH Image. Blastopore/embryo surface area ratio was calculated every 6 minutes, in 8 separate experiments, with each experiment including control and experimental embryos. Typical movie length was 4-5 hours. Embryos were rejected for analysis if the blastopore became obscured due to embryo rotation or exo-gastrulation.

Optical flow analysis of time-lapse movies

Motion of embryonic surface features was assessed by optical flow analysis (Barron et al., 1994), which estimates the velocity field within an image from frame-to-frame changes in local intensity. Movies were screened to identify heavily pigmented embryos that provide appropriate image contrast for optical flow calculations. Optical flow estimates were generated using the Lucas and Kanade algorithm (Lucas and Kanade, 1981), implemented by the FlowJ plugin (http://bij.isi.uu.nl/flowj.htm) (Abramoff et al., 2000) for ImageJ (http://rsb.info.nih.gov/ij/). The resulting flow fields for selected frames within the time-lapse movies were visualized using DC format spot noise also implemented by the FlowJ plugin. In these images color is used to code the direction of flow. All images depict dorsal to the right.

Statistics

To evaluate blastopore phenotypes within a day of experiments, blastopore areas from different conditions were statistically evaluated with a Kruskal-Wallis non-parametric ANOVA, with a 5% significance level for Dunn's multiple comparison post-test, with comparisons between all conditions. Where individual comparisons are made in the text between two conditions (e.g. control versus ventral), the significance values reported are always from ANOVAs calculated, as above, for all conditions performed in that experiment. All calculations were performed using GraphPad Prism version 4.0a for Macintosh (GraphPad Software, San Diego, CA). Embryo images presented are representative of the mean (black bar in image), except in Fig. 8, where the images correspond to the final time point.

Results

We collected a 3D digital normal series of *Xenopus* gastrulae (Fig. 1), using surface imaging microscopy (SIM) (Ewald et al., 2002). The series spanned each stage of gastrulation, from blastula through neurula, and included multiple embryos for each stage. The progress of archenteron elongation and inflation, mesendoderm mantle closure, and blastopore closure are evident at each stage (Fig. 1A-F).

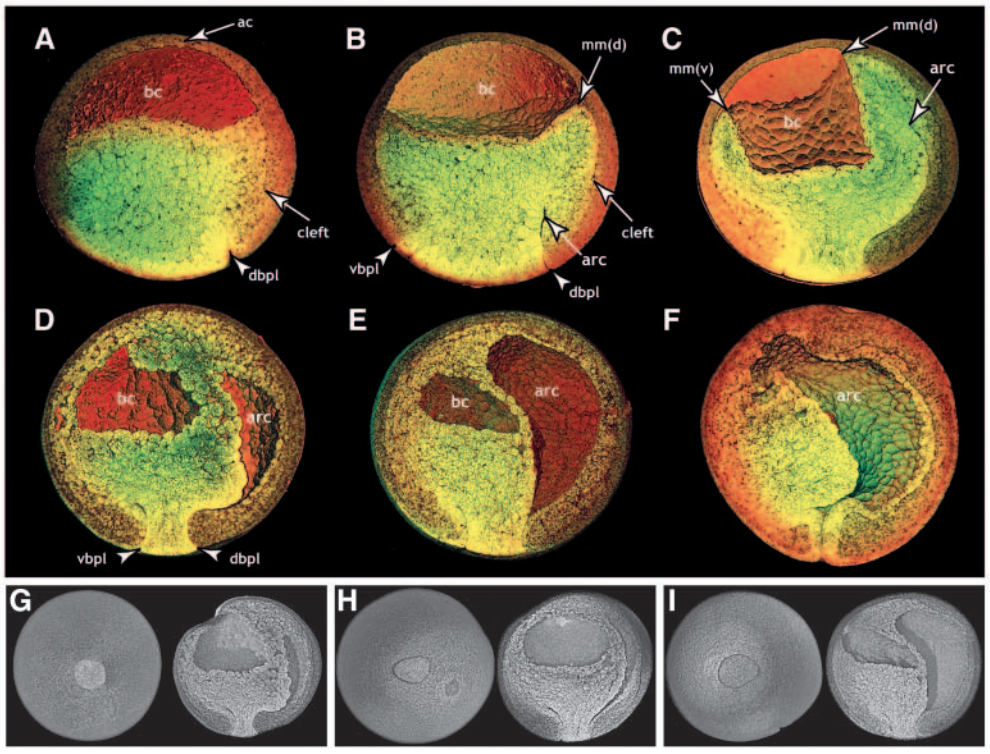

Fig. 1. Three-dimensional views of normal frog development. Normal embryos from gastrulation stages are presented in mid-sagittal view. Internal events of gastrulation are clearly visible, including blastopore groove formation (A), archenteron formation (B), archenteron elongation (C) and archenteron inflation (D-F). Mesendoderm migration over the blastocoel roof initiates on the dorsal side (A), and spreads laterally (B) and ventrally (C) before meeting at the animal pole. In a corresponding manner, the blastocoel shrinks and shifts ventrally. (G-I) Three embryos with very similar blastopores, but with significantly different degrees of archenteron elongation. bc, blastocoel; ac, animal cap; dbpl, dorsal blastopore lip; cleft, cleft of Brachet; vbpl, ventral blastopore lip; arc, archenteron; mm, mesodermal mantle; v, ventral; d, dorsal.

Beyond providing an excellent platform for observing the detailed morphology of the gastrula, the digital nature of this normal series enabled rapid evaluation of different perspectives within the same embryo (see Movie 1 in supplementary material). Surprisingly, these datasets revealed that the degree of blastopore closure was only loosely correlated with either mesendodermal mantle movement or archenteron elongation (Fig. 1G-I). At late gastrula stages, the blastopore appeared to be similar in embryos with radically different progress in archenteron elongation, archenteron inflation, mesendoderm migration and blastocoel displacement (Fig. 1G-I). Conversely, we also identified embryos with near identical archenterons and vastly different blastopores (data not shown). These observations prompted us to develop a set of morphometric measurements to allow us to investigate the apparent dissociability of internal and external gastrulation events.

Quantifying the events of gastrulation and the role of Xdsh

To quantify gastrulation events, we used obvious landmarks within the embryo, and quantified the events of gastrulation with ratios and angles that eliminate the confounding influence of natural variations in embryo size from clutch to clutch.

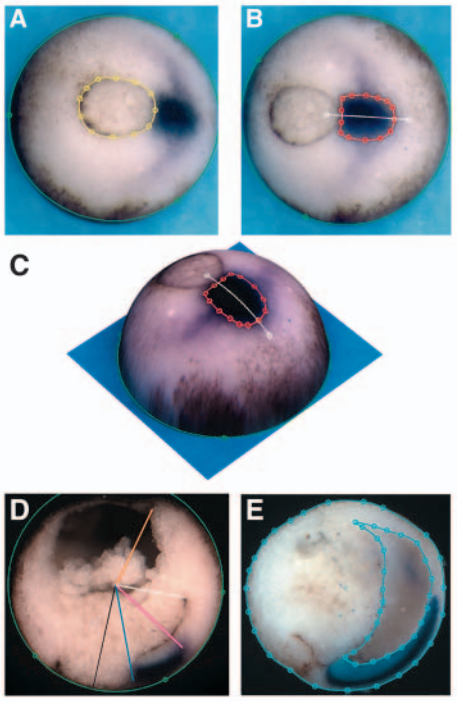

Fig. 2. Metrics for quantifying gastrulation. (A) Blastopore closure: ratio of the blastoporal surface area (yellow) to the surface area of the vegetal hemisphere (green) of the embryo. (B) Convergent extension: length-to-width ratio of the Xnot domain (red outline). (C) Spherical approximation to the embryonic surface visualized by reprojecting the 2D image into 3D. White lines in B and C indicate the dorsal midline. (D) Archenteron measurement: distance in degrees between the dorsal lip of the blastopore (blue line) and the anterior limit of the archenteron (white line); degrees of arc between the anterior limit of the *Xnot* domain (pink line) and the anterior limit of the archenteron (white line); degrees of arc between the dorsal mesendodermal mantle (orange line) and the center of the blastopore. (E) Archenteron inflation: area of the archenteron at the mid-sagittal plane divided by the area of the embryo at that plane.

We measured progress in blastopore closure by calculating the surface area occupied by the blastopore and dividing it by the area of the vegetal hemisphere of the embryo to generate a blastopore surface area/embryo surface area ratio (Fig. 2A) (see also Nakatsuji, 1974). Surface areas were inferred from the 2D projected areas by reprojection to the estimated spherical embryo surface in 3D, as described in Materials and methods (Fig. 2C); 0.0 indicates complete closure and 1 indicates a blastopore covering the hemisphere.

To assess the extent of convergent extension of dorsal tissues, we processed embryos for in situ hybridization to the *Xnot* transcript, which marks the dorsal midline tissues: notochord, floorplate and hypochord (von Dassow et al., 1993). We then measured the length-to-width ratio (LWR) of this expression domain, as it appears on the surface of the embryo (Fig. 2B,C).

Quantifying convergent extension in intact embryos is difficult because the marginal zone folds in upon itself during gastrulation. However, in a large normal series, our values for *Xnot* LWR increased as gastrulation advanced, and the increasing values for Xnot LWR showed a very significant (P<0.001) correlation to decreasing values for blastopore closure (see Fig. 3D, below), indicating the coordinate progress of these two morphogenetic events. To further test the validity of our metric, we also measured the progress in convergent extension by measuring the length of the *Xnot* domain, in degrees, as viewed on the mid-sagittal plane (Fig. 2D); this alternate formulation resulted in identical P values for all comparisons illustrated in Fig. 3. Finally, the normal progress of convergent extension, as gauged by *Xnot* LWR, was severely inhibited by expression of Xdd1 (Fig. 3A,B), which is known to block convergent extension in dorsal marginal zone explants (Sokol, 1996; Wallingford et al., 2000). Together, these data suggest that the LWR of the Xnot domain provides an effective gauge of the progress of convergent extension in intact embryos.

Xdsh signaling is required for convergent extension and blastopore closure, but not for mesendoderm internalization

We then quantified blastopore closure in the same set of embryos for which we had measured convergent extension. As expected, we found that overexpression of Xdd1 in all four blastomeres at the four-cell stage (circumferential expression) resulted in significantly deficient blastopore closure (Fig. 3C; P<0.001, n=113 control and 70 circumferential, four independent experiments). Plotting each embryo based on its degree of blastopore closure and convergent extension reveals a strong correlation between the degree of convergent extension and blastopore closure (Fig. 3D).

We next sought to understand the consequences of defective Xdsh signaling on other aspects of gastrulation. To achieve this, we imaged dorsally injected embryos using SIM. In these digital datasets, we observed open blastopores, but we were intrigued by the consistent presence of excess material immediately inside the blastopore lip (Fig. 4). In control embryos viewed in sagittal section, the marginal zone appears as a sheet that smoothly curves animalward from the blastopore (Fig. 4A). By contrast, in Xdd1-injected embryos, the marginal zone appears as a rounded ridge at the blastopore lip that

gradually thins away from the lip (Fig. 4B, red arrowhead). Taking advantage of our SIM digital datasets, we evaluated the radial extent of internalized material in Xdd1-injected embryos. The ridge was still observed after rotating our digital datasets 30° in either direction from mid-sagittal (Fig. 4b′, red arrowhead), suggesting that internalization of marginal zone material had occurred in at least a 60° arc on the dorsal side of this Xdd1-injected embryo.

To confirm that this ridge of material represented involuted marginal zone, we examined *Xnot*-staining in Xdd1-overexpressing embryos. The ridge of material inside the dorsal lip of these embryos was consistently Xnot-positive (Fig. 4D, red arrowhead), indicating that marginal zone material had involuted. As we know that these same embryos failed to undergo convergent extension or blastopore closure (Fig. 4C,D; yellow and green arrowheads; and see Fig. 3, above), this result indicates that the internalization of this *Xnot*-positive material is independent of both convergent extension and blastopore closure.

Because blastopore closure is commonly thought to be tightly coupled to mesendoderm internalization, we studied gastrulation of normal and Xdd1-injected embryos in time-lapse movies. In control embryos, the involution of marginal zone material began dorsally and proceeded to the

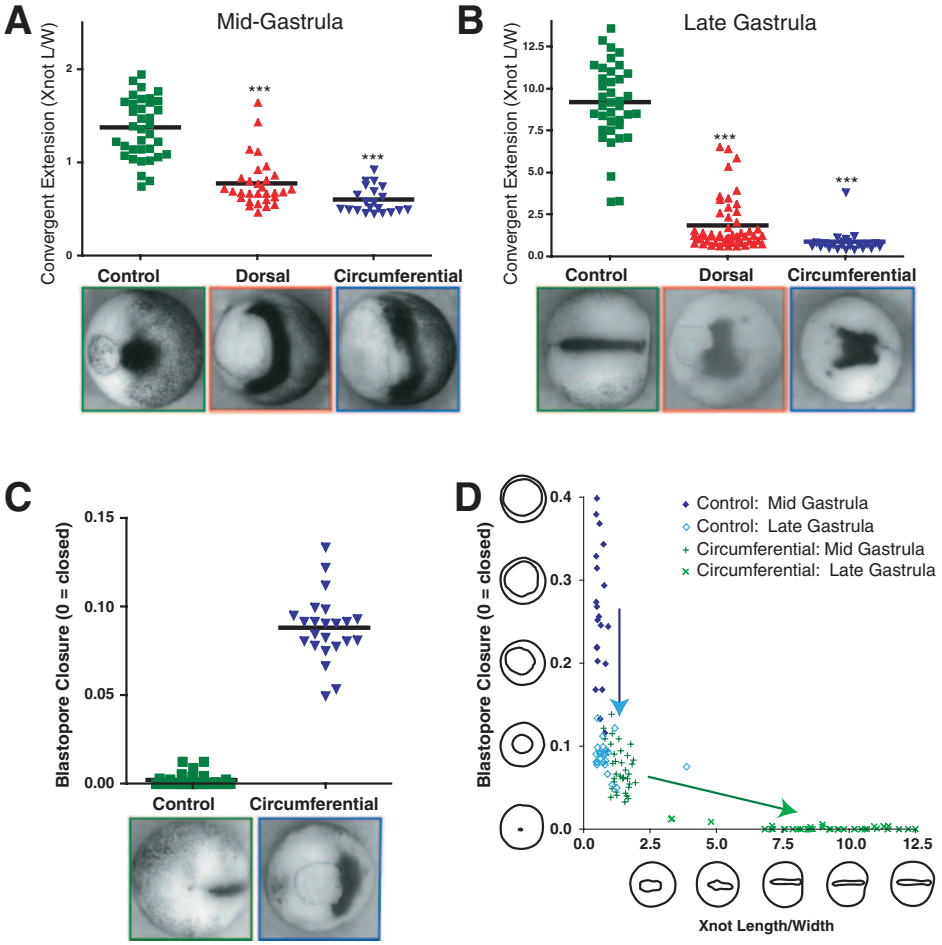

Fig. 3. Effects of Xdd1 on convergent extension and blastopore closure. (A) Convergent extension measurements at mid-gastrulation. (B) Convergent extension measurements at mid-gastrulation (***P<0.001; four experiments; n=113 control, 109 dorsal, 70 circumferential). (C) Blastopore closure measurements at mid-gastrula stage (P<0.001, four experiments; n=113 control, 70 circumferential). (D) Plot of convergent extension versus blastopore closure. Each point repesents one embryo.

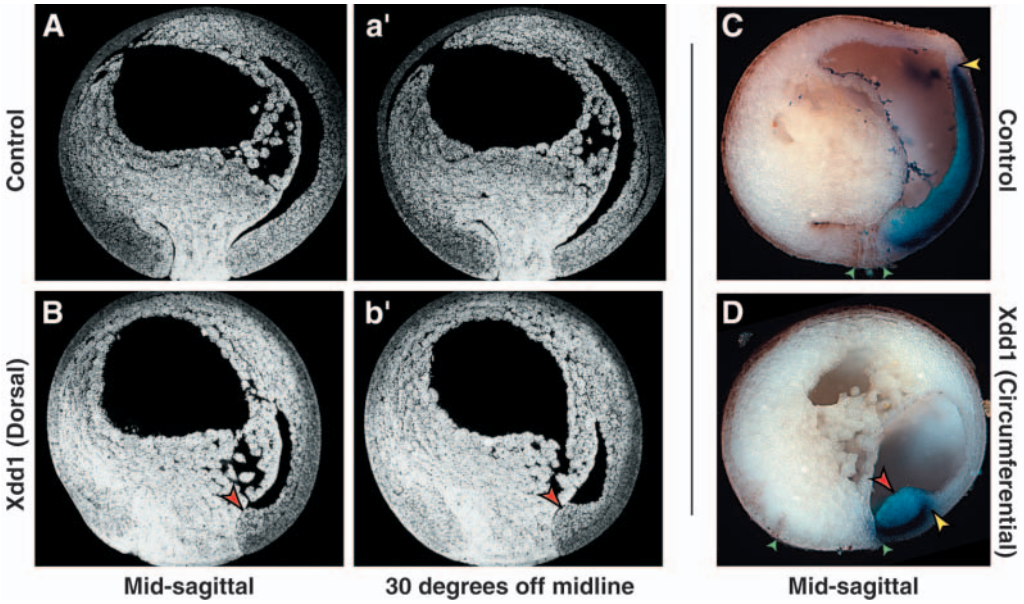

Fig. 4. Marginal zone internalization in Xdd1-expressing embryos. (A) Mid-sagittal plane of SIM dataset of a control embryo. (a′) Section from the embryo shown in A, 30° off mid-sagittal. (B) Mid-sagittal plane of SIM dataset of a dorsally injected Xdd1 embryo. (b′) Section from the embryo shown in B, 30° off from mid-sagittal. (C) Mid-sagittal view of a control embryo hybridized to Xnot (yellow arrowhead indicates the anterior limit of Xnot staining; green arrowheads indicate blastopore lips). (D) Mid-sagittal cleavage of a circumferentially injected Xdd1 embryo hybridized to Xnot. Ridge of internalized tissue (red arrowheads) is Xnot positive.

lateral and then ventral lips of the blastopore (see Movie 2 in supplementary material). This movement is represented in Fig. 5 by optical flow diagrams. In this diagram, the colors indicate the direction of movement (see index; Fig. 5C) and the length of the lines corresponds to the speed of movement. Material moving from the surface of the embryo to the interior, at the blastopore lip, is indicated by regions of opposed flow (white boxes in Fig. 5a′). In control embryos, the internalization of surface material from the marginal zone was always accompanied by a coordinate internalization of yolk plug material under the lip of the blastopore (Fig. 5a′; Movie 2). The internalization of yolk plug cells also began dorsally and propagated ventrally (Fig. 5a′; Movie 2).

Internalization of marginal zone material was observed in time-lapse movies of Xdd1-injected embryos that display almost no blastopore closure (see Movie 3 in supplementary material; Fig. 5b′,D,d′). Optical flow analysis demonstrates that internalization of the marginal zone, and coordinate internalization of the yolk plug cells, begins dorsally and sweeps ventrally as gastrulation proceeds, even though blastopore closure stalls in these severely affected embryos (Fig. 5b′). Tracings of individual cells from time-lapse movies confirm internalization of both marginal zone and yolk plug tissues in Xdd1-expressing embryos with essentially no blastopore closure (Fig. 5D,d′).

Blastopore closure requires Xdsh function in both ventral/lateral and dorsal marginal zone tissues

The finding that both marginal zone and yolk plug internalization proceeds in embryos with disrupted Xdsh signaling suggested that the mechanisms of internalization and blastopore closure are not tightly coupled. Because we observed that Xdsh is required for blastopore closure, we next sought to better define this requirement. We tested the regional requirements for Xdsh activity in blastopore closure by performing targeted injections of Xdd1 into the two dorsal, the two ventral, or all four cells (circumferential) at the four-cell stage. These injections produced a graded series in severity, with increasing effect when injected in the ventral, dorsal, or all four cells. Xdd1 had the greatest effect when expressed circumferentially, but all three experimental conditions were significantly different statistically from control embryos (Fig. 6, $P<0.001$). The ventral requirement is apparent at the mid-gastrula stages, indicating an early role for Xdsh in the ventral/lateral marginal zone.

To examine the effect of disrupted Xdsh signaling on the timing and dynamics of blastopore closure, we collected time-lapse movies of blastopore closure in dorsally, ventrally or circumferentially injected embryos. These movies reveal increasingly severe defects in blastopore closure from ventral to dorsal to circumferential injections (Fig. 7; see Movies 4-7 in supplementary material). Moreover, the time-lapse analysis confirmed that the defects in blastopore closure are evident early in gastrulation; the difference between the conditions is sharpest at the middle of gastrulation (Fig. 8A,B). In all cases, some closure occurs, and most of this closure occurs in the second half of gastrulation (Fig. 8A,B). In some of the more severely affected dorsal and circumferential embryos, we observed a stalling, or even a slight opening of the blastopore, followed by a sudden closing movement (Fig. 8B, circumferential; see Movie 7). This behavior was typically accompanied by a mismatch in the internalization of the yolk plug and surface material. When the yolk plug began rotating towards the blastopore lip, without accompanying surface movements, the blastopore would stall or open slightly. The sudden partial closure was correlated with the onset of internalization of surface material.

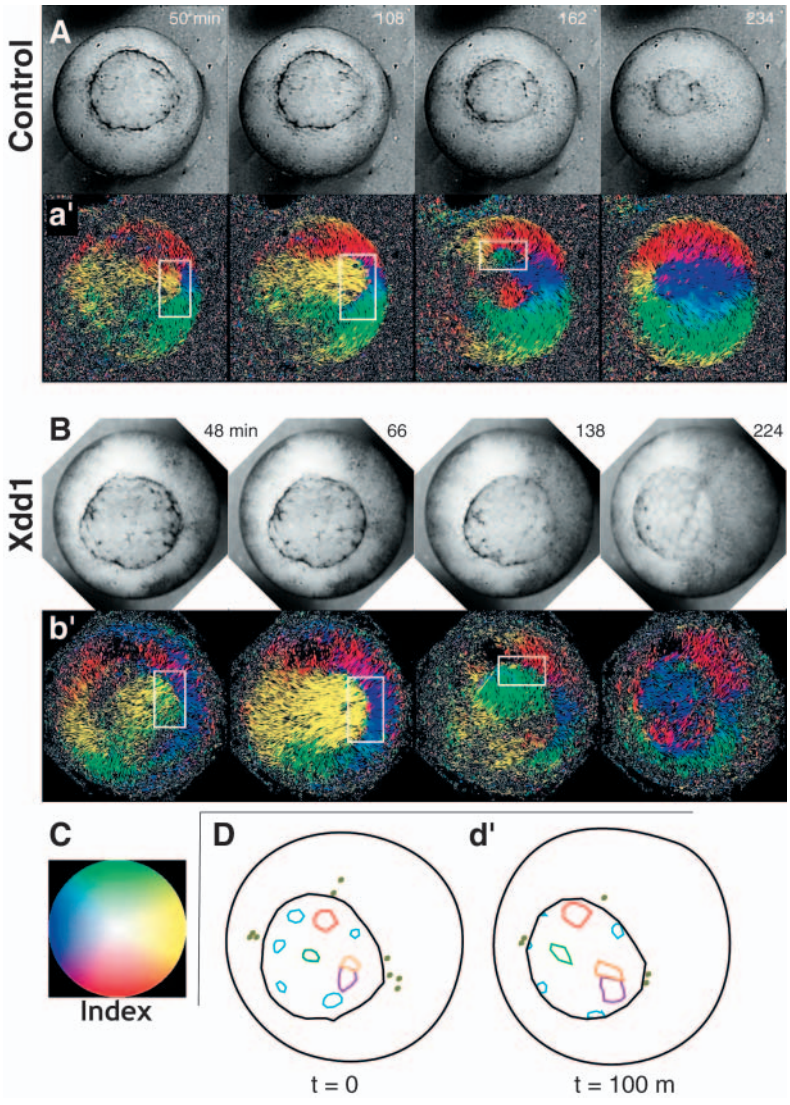

Fig. 5. Marginal zone internalization without blastopore closure in Xdd1-expressing embryos. Optical flow analysis of control (A; see Movie 2 in supplementary material) and Xdd1-injected (B; see Movie 3 in supplementary material) embryos. As indicated in the key in panel C, color denotes the direction of flow in a′ and b′ (e.g. yellow lines indicate dorsal movement; blue lines indicate ventral movement). Opposed flow (e.g. yellow meeting blue) represents internalization and is highlighted with white boxes. Cell tracings of Xdd1-injected embryos (D,d′) also reveal the internalization of cells in both the marginal zone and yolk plug.

Together, these data demonstrate that blastopore closure requires Xdsh signaling in both the dorsal and the ventral marginal zones, and that the requirement for Xdsh in blastopore closure is most significant during the middle gastrula stages.

Archenteron elongation requires Xdsh signaling during early gastrulation but not during late gastrulation

To assess the role of Xdsh signaling in archenteron development, we measured the degrees of arc between the dorsal lip of the blastopore and the anterior limit of the archenteron (Fig. 2D) (see also Moore, 1946). Archenteron inflation was also estimated as the 2D area of the archenteron divided by the area of the embryo, both as viewed in mid-sagittally cleaved embryos (Fig. 2E). We tested the requirement for Xdsh in archenteron formation through ventral, dorsal and circumferential injections of Xdd1 (as above). When embryos were fixed and analyzed at mid-gastrula stages, both dorsally and circumferentially injected embryos displayed a significant defect in early archenteron elongation compared with controls (Fig. 9A; P<0.001; means=79° control, 19° dorsal, 18° circumferential).

During the second half of gastrulation, the measurements showed that both control and Xdd1-expressing embryos elongate their archenterons to comparable degrees, approximately 100° (Fig. 9B). At late gastrulation, the gap between control and Xdd1-expressing embryos reflects the difference in archenteron angle established during the first half of gastrulation (compare Fig. 9A with 9B; means=191° control, 127° dorsal, 114° circumferential). Even at late gastrula stages, the archenteron lengths of both dorsal and circumferential embryos remain statistically different from those of the controls (Fig. 9B; P<0.001).

In light of the requirement for Xdsh in both dorsal and ventral/lateral tissues for blastopore closure, discussed above (Fig. 6), we tested for differences in archenteron elongation based on regionally targeted ventral, dorsal and circumferential injections. Embryos were fixed at both mid- and late-gastrula stages, and in all cases the ventrally injected embryos were statistically indistinguishable from the controls (not shown), and the dorsally injected embryos were statistically indistinguishable from the circumferentially injected embryos (Fig. 9A,B). From these data, we conclude that, in contrast to blastopore closure, PCP signaling is required only in dorsal tissues for archenteron elongation.

During late gastrula stages, the anterior portion of the archenteron expands rapidly (Keller, 1975; Keller, 1981). We measured this anterior expansion as the degrees of arc between the anterior limit of the *Xnot* domain and the anterior end of the archenteron (Fig. 2D). We observed no significant difference in the amount of anterior archenteron between control and Xdd1-injected embryos (Fig. 9C), further supporting the independence of archenteron elongation from convergence and extension during the second half of gastrulation (Fig. 9B).

To assess later archenteron development, we injected

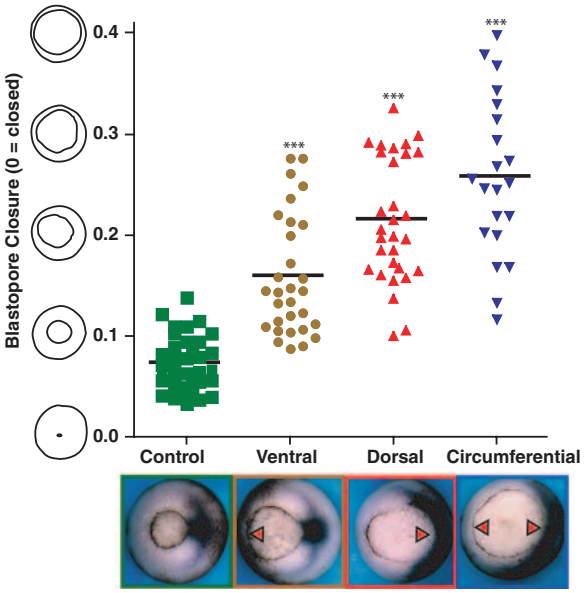

Fig. 6. Xdsh is required in ventral/lateral and dorsal tissues for blastopore closure. Plot of blastopore closure in embryos expressing Xdd1 in ventral, dorsal, or all four blastomeres (circumferential) at the four-cell stage (***P<0.001, n=36 control, 30 each dorsal and ventral, 21 circumferential). Note the morphology of the blastoporal boundary in each condition; the affected side is visibly less taut in each case (red arrowheads).

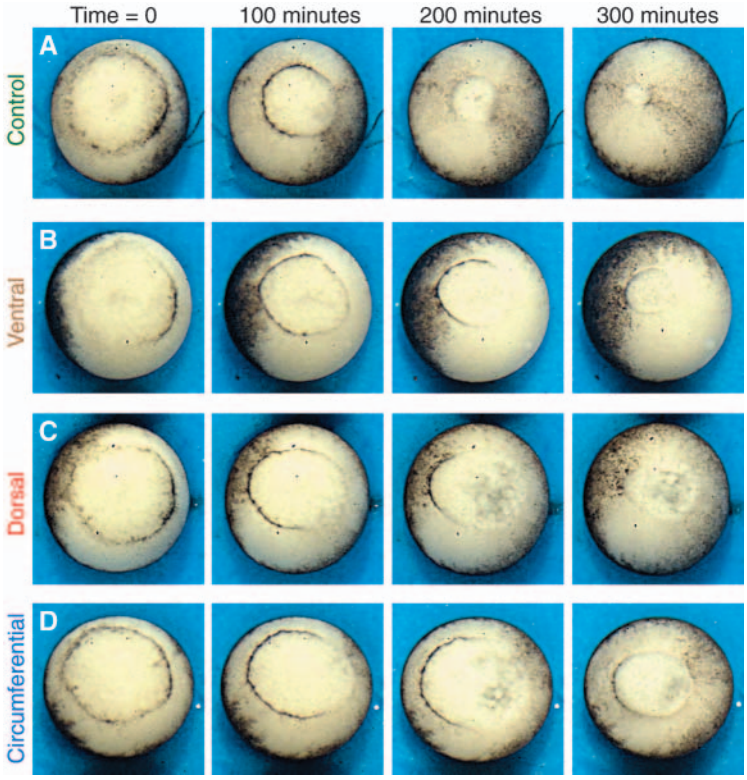

Fig. 7. Time-lapse analysis of blastopore closure in Xdd1-injected embryos. (A-D) Still frames from time-lapse movies (see Movies 4-7 in supplementary material); control (A), ventral (B), dorsal (C) and circumferential (D) embryos. Ventral, dorsal and circumferential embryos all show defects in closure. Measurements for blastopore size over time are shown in Fig. 8.

embryos with Xdd1 in the two dorsal cells, and cultured embryos to tailbud stages; SIM was used to generate 3D images of the whole embryos. These embryos had profound defects in their dorsal axes, but had relatively normal archenteron lengths, extending all the way to the head of the embryos (Fig. 10).

Archenteron inflation and elongation are separable processes

In our 3D digital renderings of gastrulae, we observed that in normal embryos the very short, early archenterons were never inflated, whereas later, longer archenterons may or may not be inflated (Fig. 1). In these datasets, archenteron elongation and inflation did not appear to be coupled (Fig. 1G-I). We measured archenteron inflation (Fig. 2E) in late gastrula embryos, and plotted inflation against elongation. At late gastrula stages, we observe a statistically significant difference (P<0.001) in archenteron inflation between controls and both dorsally and circumferentially injected embryos.

Interestingly, we saw no correlation between archenteron elongation and archenteron inflation in normal or Xdd1-injected embryos (Fig. 11B). For a given length of archenteron, a huge spread of values for inflation can be found. Also, we

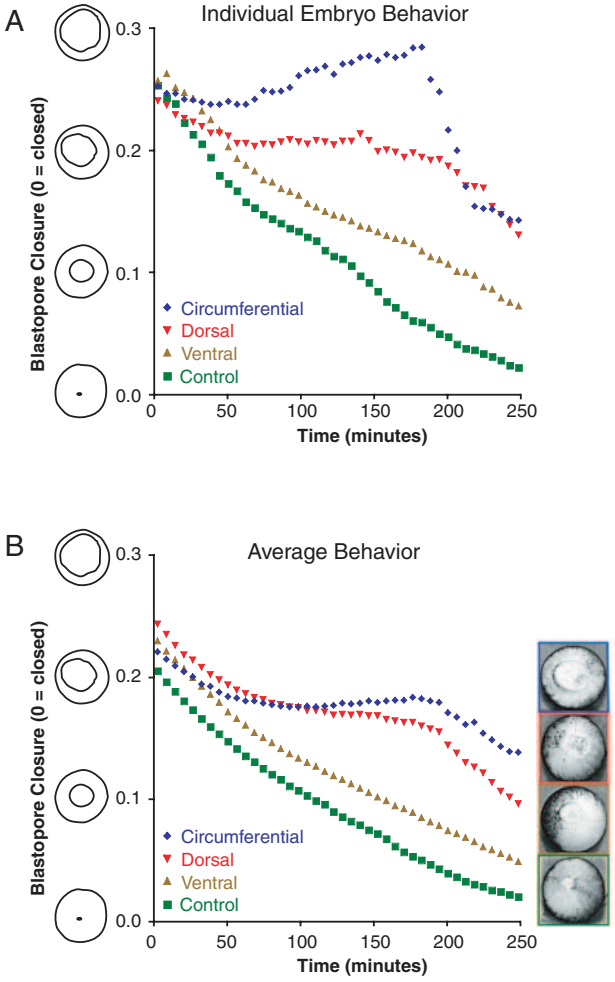

Fig. 8. Kinetics of blastopore closure in Xdd1-injected embryos. (A) Kinetics of closure for the embryos shown in Fig. 7A-D. (B) The mean kinetics of closure for eight independent blastopore closure experiments (n=20 control, 12 ventral, 11 dorsal, 16 circumferential). Within each day, and on average, we observed increasingly severe defects in blastopore closure in ventrally, dorsally and circumferentially injected embryos.

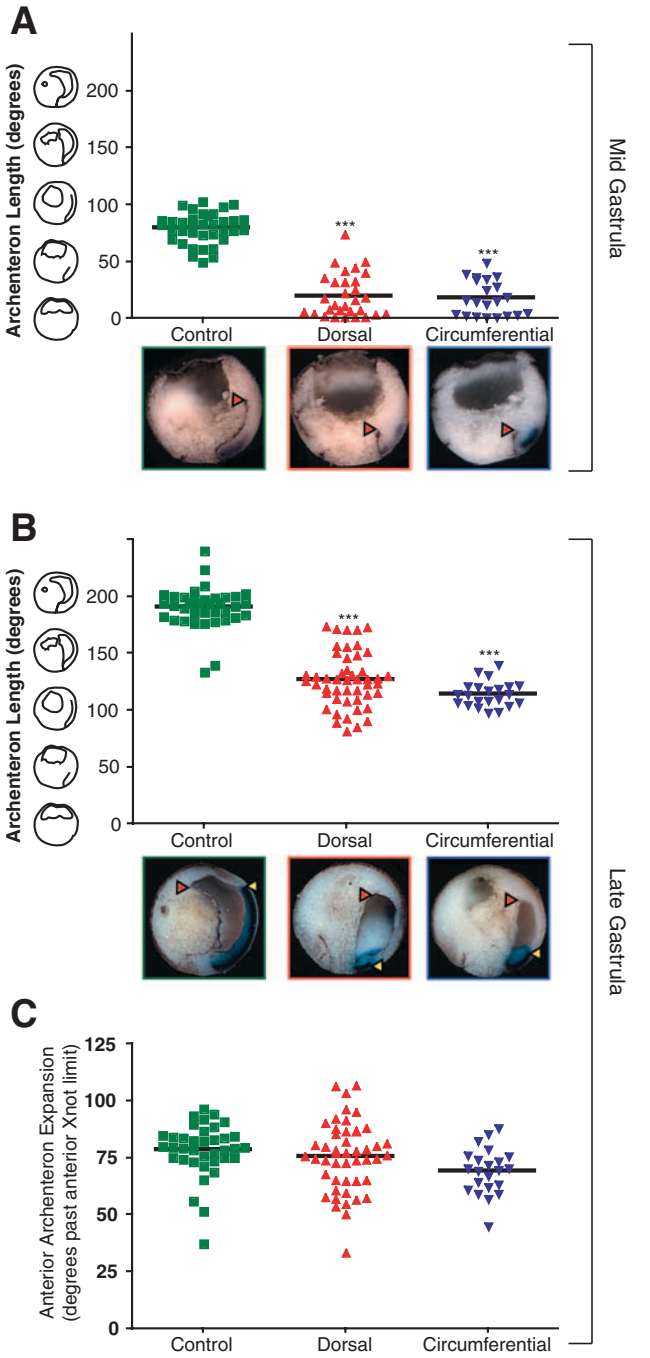

Fig. 9. Archenteron elongation requires Xdsh function during early but not late gastrula stages. Archenteron elongation is disrupted in dorsally and circumferentially injected embryos at mid-gastrula (A) (***P<0.001; n=36 control, 30 dorsal, 21 circumferential) and late-gastrula (***P<0.001; n=38 control, 52 dorsal, 23 circumferential) stages. The fraction of the archenteron (red arrowhead at anterior limit) overlain by the *Xnot* domain (yellow arrowhead) is very different between control and experimental embryos, demonstrating that the lengthening of the archenteron is proceeding in the absence of convergent extension. (C) Archenteron anterior expansion is not statistically different between Xdd1-injected embryos, at late gastrula stages.

observed that the circumferentially injected embryos have less inflation (P<0.01) than do those injected dorsally (Fig. 11A). As dorsally injected embryos are not significantly different from circumferentially injected embryos in archenteron length (Fig. 9B), these findings support the idea of dissociability between archenteron elongation and inflation.

It has been suggested that the archenteron expands through the direct transfer of fluid from the blastocoel (Tuft, 1965; Zotin, 1965). Indeed, cavities between the blastocoel and the archenteron are often observed in sections and in cleaved embryos (Fig. 12A,B). We confirmed that such cavities were not the result of cleavage or sectioning artifacts, by identifying such cavities in intact *Xenopus* embryos using magnetic resonance imaging (MRI) and confocal microscopy (Fig. 12C and data not shown).

To determine whether or not such cavities could connect the blastocoel to the archenteron, we used the high-resolution 3D datasets obtained by SIM to generate volume renderings of cavities within a late gastrulae frog embryo. These volume renderings revealed connections linking such cavities to both blastocoel and archenteron (Fig. 12D,E; see Movie 8 in supplementary material).

Mesendoderm extension appears to be independent of Xdsh signaling

The mesendodermal mantle moves animal-ward along the roof of the blastocoel in a hemispherical wave (Davidson et al., 2002). Although it can be difficult to assay the exact position of the leading edge of the mesendoderm, we measured the progress of mesendoderm extension in degrees of arc (Fig. 2D). At mid-gastrula stages, we observed only a very modest difference in mesendoderm progress in dorsally injected Xdd1 embryos (P<0.05; control, 173°; dorsal, 161.5°). In circumferentially or ventrally injected embryos, we saw no significant difference (P>0.05; control 173°; ventral, 179°; circumferential 163.2°). By the end of gastrulation, the mesendodermal mantle had closed at the animal pole in all injected embryos. This result suggests that Xdd1 does not generally inhibit cell motile behaviors, and is consistent with the normal development of anterior structures in Xdd1-injected embryos (Sokol, 1996).

Dissociability of morphogenetic processes during *Xenopus* gastrulation

Examination of SIM datasets (Fig. 1G-I) indicated that blastopore size is a poor indicator of the internal progress of gastrulation. To quantify the normal variability in gastrulation, we plotted a normal series of embryos such that each embryo is a single point plotted for both archenteron progress and

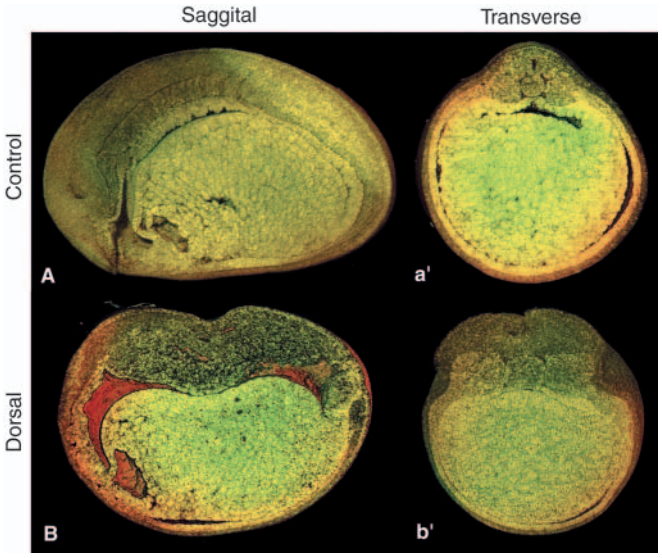

Fig. 10. Late archenteron formation in Xdd1-injected embryos. (A) Sagittal view of a tailbud stage control embryo imaged using SIM. (a′) Tranverse view of the embryo shown in A. (B) Sagittal view of a tailbud stage Xdd-1 injected embryo imaged using SIM. (b′) Tranverse view of the embryo shown in B. Despite severe disruption of convergent extension in the dorsal axis, the archenteron forms and elongates to cover the entire head-to-tail length.

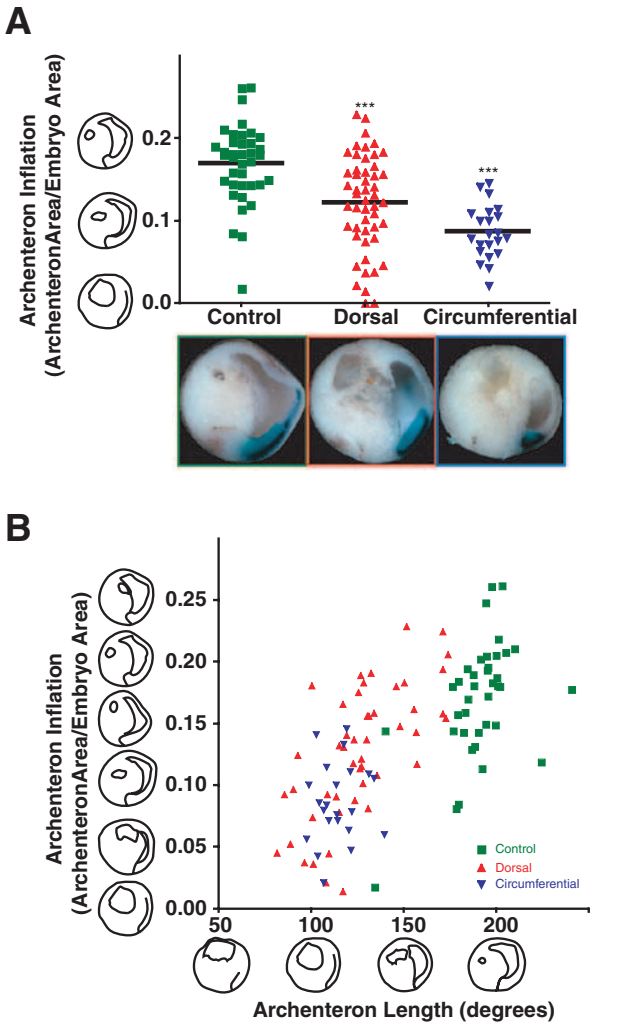

Fig. 11. Effects of Xdd1 on archenteron inflation. (A) Archenteron volume is reduced significantly in both dorsally and circumferentially injected embryos (***P<0.001, n=38 control, 50 dorsal, 24 circumferential). In contrast to archenteron length, archenteron volume is significantly reduced in circumferentially injected embryos compared with in dorsally injected embryos (**P<0.01). (B) A plot of archenteron inflation against archenteron elongation shows no obvious correlation between the two processes (each point represents a single embryo).

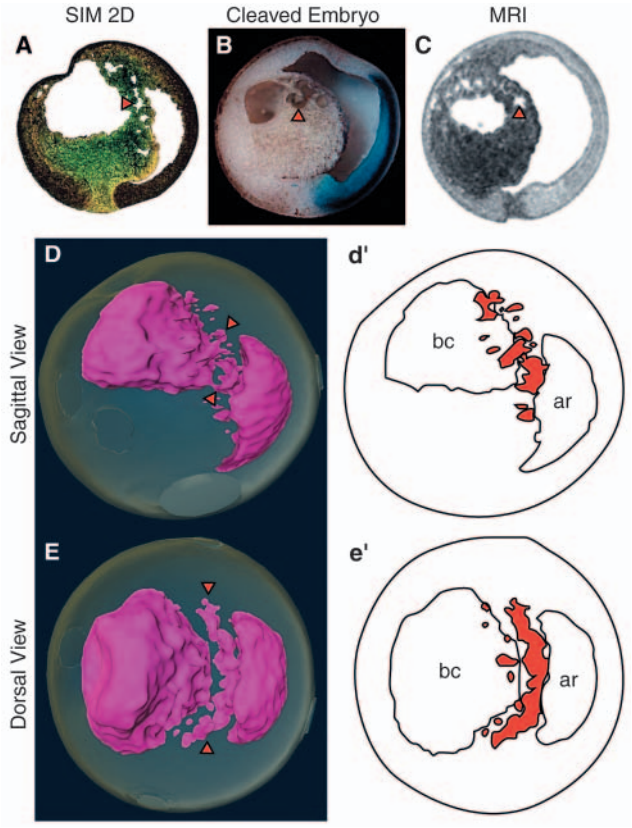

Fig. 12. Archenteron inflation by fluid transfer from the blastocoel. (A-D) Cavities between the blastocoel and the archenteron were visualized with SIM (sagittal section, A), in cleaved embryos (B), and with MRI (sagittal section of intact embryo, C). (D) Sagittal view of the SIM dataset from A rendered to visualize internal spaces, highlighting (red arrowheads) the cavities connecting the blastocoel and archenteron. (E) Transverse volume render of the SIM dataset from A. Cavities are highlighted in red in the tracings shown in d′ and e′. An animation of this volume rendering is presented in Movie 8 in supplementary material.

blastopore progress (Fig. 13A). As a reference, we plotted the Niewkoop and Faber normal stages on the same graph, with the width of the circle corresponding to the approximate predicted range of variability (10° of arc) (Nieuwkoop and Faber, 1994). We observed a much higher degree of variability than had been previously described; for example, for a given blastopore size, embryos can have almost 100° of arc difference in the extent of archenteron elongation (Fig. 13). For a single given archenteron length, blastopore size can indicate stage 10.5 through stage 12 (Fig. 13).

To determine the extent to which observed deficits in blastopore closure and archenteron elongation correlated with the severity in the block of convergent extension, we plotted each of these values for individual early and late gastrulae. By late gastrula stages, the control embryos have elongated their archenterons, and have converged and extended greatly (green squares shifted up and to the right in Fig. 14a′ relative to in Fig. 14A). By contrast, the circumferentially injected siblings proceed in archenteron elongation with essentially no convergent extension (blue triangles shifted straight up in Fig. 14a′ relative to in Fig. 14A). Dorsally injected embryos show a roughly similar behavior. We conclude from these paired observations that there are at least two distinct processes driving elongation of the archenteron, one, which occurs early, is dependent on Xdd1 signaling and correlates temporally with convergent extension. The second elongation mechanism is independent of Xdsh signaling, can occur in the absence of convergent extension, and appears to occur later in gastrulation than the Xdd1-dependent mechanism.

To test the coupling between archenteron elongation and blastopore closure, we plotted the same embryos according to their progress in these parameters (Fig. 14B). From mid to late gastrula stages, embryos of all conditions make significant progress in both processes (all marks shifted up and right in Fig. 14b′ relative to in Fig. 14B). There is a statistically significant deficit in both archenteron elongation and blastopore closure, in all injected embryos. There is also a highly significant difference ($P<0.001$) between dorsally and circumferentially injected embryos in their blastopore closure values, but not in their archenteron elongation values (Fig. 14b′). This discrepancy reflects a requirement for Xdsh signaling in the dorsal blastomeres for blastopore closure and archenteron elongation. Conversely, Xdsh signaling in the ventral blastomeres is required for blastopore closure, but is dispensable for archenteron elongation.

Discussion

Recent studies of gastrulation have focused on the identification of the important molecules involved, and to a lesser extent on the role that these molecules play in controlling discrete cell behaviors. Less attention has been paid recently to the embryological mechanisms by which the blastopore closes, by which the marginal zone is internalized and the embryo surface is covered with ectoderm, and by which the archenteron is formed. Here, we present 3D digital datasets of *Xenopus* gastrulae that allow the observation of the same embryo from all aspects (Fig. 1), and we describe simple metrics for quantifying gastrulation events (Fig. 2). Combining these approaches with time-lapse microscopy, we find that the signaling molecule Dishevelled is required for blastopore closure, but not for mesendoderm and yolk plug internalization (Figs 3-5). We show that blastopore closure requires intact Xdsh signaling in both dorsal and ventral marginal zone cells (Figs 6, 7). We also show that Xdsh is required for archenteron elongation during early gastrulation stages, but not for the anterior expansion of the archenteron during late gastrulation. Our data also reveal a separability of archenteron elongation and inflation (Figs 9-12). Finally, we present quantification of the variability within a given gastrulation process, and of the degree of coupling between the events in *Xenopus* gastrulae (Figs 13, 14).

Convergent extension, marginal zone internalization and blastopore closure

One current model of blastopore closure suggests that convergent extension movements, which begin on the dorsal side of the marginal zone and propagate ventrally, generate arcs of hoop stress that are shortened progressively as the behaviors propagate (Keller et al., 2003). This progressive arc-shortening is thought to progressively constrict the blastopore, thereby internalizing the marginal zone (Keller et al., 2003; Keller and

Jansa, 1992; Shih and Keller, 1992b; Shih and Keller, 1994). Alternately, it has been suggested that blastopore closure and marginal zone internalization may be separable (Phillips, 1984), and internalization of at least ventrolateral material in the absence of dorsal convergent extension has been previously shown in microsurgical experiments (Schectman, 1942). Indeed, more recent studies indicate that much internalization occurs through the combined action of vegetal rotation movements and the active internalization of individual cells (Ibrahim and Winklbauer, 2001; Winklbauer and Schurfeld, 1999).

Because defective blastopore closure was consistently correlated with defective convergent extension in our Xdd1-injected embryos (Fig. 3), our data support the progressive arc-shortening model of blastopore closure. Furthermore, the presence of compact, internalized marginal zone material in embryos with defective blastopore closure (Fig. 4) is consistent with the notion that it is convergent extension of post-involution material that drives the vegetalward movement of the blastopore lip (Keller, 1984; Keller et al., 1985). However, blastopore closure can be accomplished without convergent extension in UV-irradiated *Xenopus* embryos (Cooke, 1985; Gerhart et al., 1989; Malacinski et al., 1977). In these cases, other tissue movements, such as convergent thickening (Keller and Danilchik, 1988), are thought to drive blastopore closure. This fact leaves open the possibility that Xdsh is also required for the other processes that contribute to blastopore closure in *Xenopus*. Further study will be necessary to discern the role of Xdsh in these other processes.

In addition, the ability of Xdd1-injected embryos to reduce their blastopore area to some degree (Figs 7, 8) implies that other, Xdsh-independent cellular mechanisms contribute to blastopore closure as well. One such mechanism could be the evacuation of marginal zone cells from the blastopore lip and insertion of these cells into the lining of the cleft of Brachet (Ibrahim and Winklbauer, 2001). This model also helps to explain the observed separability of marginal zone and yolk plug internalization from blastopore closure. We consistently observe robust, internalization of both marginal zone and yolk plug tissue during gastrulation in embryos in which the blastopore is not closing (see Movies 2-7 in supplementary material, Fig. 5).

Together, our data suggest that vegetal rotation and active involution are the primary motors of mesoderm

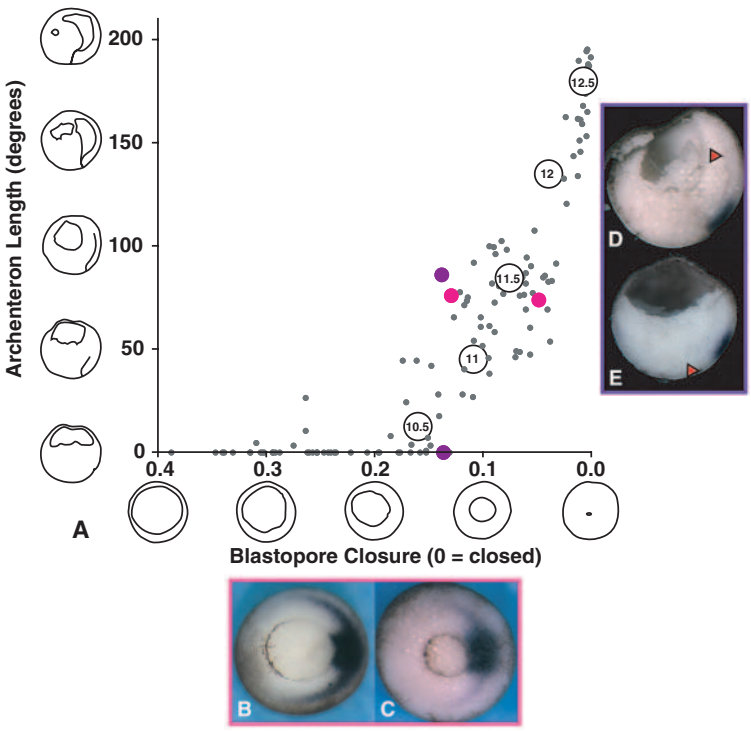

Fig. 13. Dissociability of archenteron elongation and blastopore closure. (A) Plot of blastopore closure versus archenteron elongation for 97 normal embryos of various gastrula stages. (B,C) Embryos with highly similar archenterons and very different blastopores, indicated in A with pink points. (D,E) Embryos with highly different archenterons and very similar blastopores, indicated in A with purple points. The anterior limit of the archenteron is indicated with a red arrowhead. Nieuwkoop and Faber standard stages are presented for reference (Nieuwkoop and Faber, 1994), with the size of the circles approximately corresponding to the predicted variability.

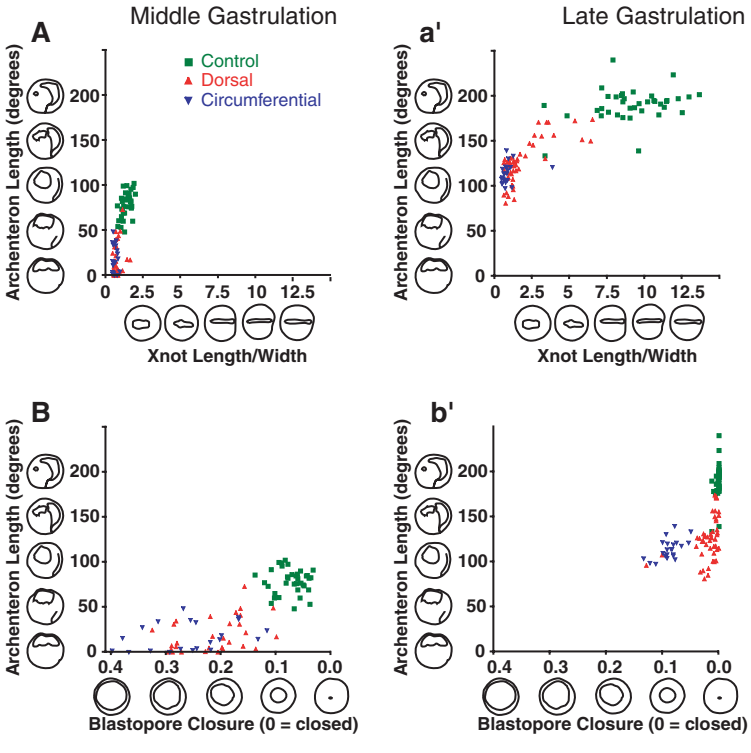

Fig. 14. Uncoupling of blastopore closure and archenteron elongation. (A,a′) Embryos fixed at mid (A) and late (a′) gastrula stages are plotted to show the combined progress in both convergent extension and blastopore closure. (B,b′) Embryos fixed at mid (B) and late (b′) gastrula stages are plotted to show the combined progress in both blastopore closure and archenteron elongation. Xdd1-injected embryos make essentially no progress in convergent extension between the two time points, but progress significantly in both blastopore closure and archenteron elongation.

internalization throughout the gastrula embryo, with convergent extension contributing only a small amount to internalization. Conversely, we argue that post-involution convergent extension is the primary motor driving the closure of the blastopore, with active involution contributing relatively little. Further studies into the molecular and cellular mechanisms driving these events of gastrulation will be required for a clear understanding to emerge.

An important role for Xdsh in the ventrolateral marginal zone during blastopore closure

Although often ignored, cells of the lateral – and to a lesser degree the ventrolateral – marginal zone do engage in modest convergent extension during the second half of gastrulation (Keller and Danilchik, 1988). Our data indicate that these ventrolateral cells make an important contribution to blastopore closure in an Xdsh-dependent manner (Figs 6-8). This contribution of ventrolateral cells to blastopore closure may help to explain the ability of embryos ventralized by UV irradiation to close their blastopore (Cooke, 1985; Gerhart et al., 1989; Malacinski et al., 1977).

Although the cells of the ventrolateral marginal zone undergo only limited convergent extension, they may also contribute mechanically to events driven on the dorsal side. Ventral marginal zone cells make stable, if not polarized, contacts with neighboring cells throughout gastrulation (Reintsch and Hausen, 2001). Stable attachments such as these may contribute to the establishment of tension around the circumference of the marginal zone. In fact, relaxation of such tension lines by microsurgical manipulation perturbs gastrulation and results in abnormally open blastopores (Beloussov et al., 1975; Beloussov et al., 1990). Furthermore, it has been shown that relaxation of the circumferential tension in the marginal zone can reduce the efficacy of cell intercalations (Beloussov et al., 1990; Beloussov et al., 2000). Consistent with a role for tissue tension in blastopore closure, the affected side of the blastopore in Xdd1-injected embryos appears to be visibly less taut at mid-gastrulation (Fig. 6, red arrowheads).

As we have previously shown that Xdsh is required to maintain normal lamellipodial stability (Wallingford et al., 2000), we propose that, when Xdd1 is expressed ventrally, it disrupts the stability of cellular protrusions that are important for maintaining tension within the ventral marginal zone, even at early gastrula stages when this tissue is not engaged in convergent extension, explaining the observed deficit in ventrally-injected embryos at mid-gastrula stages (Fig. 8). Later in gastrulation, the failure of these lamellipodia to polarize correctly will block ventrolateral convergent extension, further disrupting blastopore closure.

Finally, the ventral marginal zone undergoes convergent thickening during late gastrulation (Keller and Danilchik, 1988), as mentioned above. The cellular basis of convergent thickening is poorly understood, but it is clearly possible that this process could involve polarized cell behaviors that require intact Xdsh signaling.

Xdsh, convergent extension and archenteron elongation

Convergent extension of the marginal zone produces a dramatic amount of force (Moore et al., 1995), and it is tempting to speculate that most aspects of anteroposterior axis elongation during gastrulation are driven by this tissue movement. However, the relationship between convergent extension and archenteron formation has not, to our knowledge, been previously examined by direct experiment, and evidence can be found to the contrary. For example, it has been shown that in hybrids of *Rana* species in which convergent extension is defective, archenteron elongation can proceed (Gregg, 1957; Gregg and Klein, 1955; Moore, 1946). Likewise, hydrolytic sulfatase disrupts convergent extension potently, and whereas archenteron inflation is severely affected, archenteron elongation is only mildly reduced (Wallingford et al., 1997).

We show here that interfering with Xdsh signaling by Xdd1 overexpression in the dorsal tissues produced a significant defect in archenteron elongation by the mid-gastrula stage (Fig. 9) that is correlated to a defect in convergent extension (Fig. 14). However, during the second half of gastrulation, the archenteron elongates even in embryos that lack additional dorsal convergent extension (Fig. 9). Our data demonstrate that anterior archenteron expansion is Xdsh independent (Fig. 9C). Moreover, the data suggest that most of the elongation of the archenteron during late gastrula stages can be accounted for by anterior expansion and does not require convergent extension. This result implies that at least two mechanisms are required independently to elongate the archenteron. Two distinct phases of archenteron elongation have also been noted in echinoderms (Kominami and Takata, 2000). The mechanisms contributing to archenteron elongation in the second half of gastrulation remain to be determined, although several candidates exist.

The apical surfaces of bottle cells at the blastopore lip re-spread at the end of gastrulation (Keller, 1975), and manual removal of bottle cells results in a truncation of the archenteron, suggesting that re-spreading of these cells contributes to archenteron length (Keller, 1981). Likewise, disruption of epiboly by overexpression of *Xoom* mRNA (Hasegawa and Kinoshita, 2000) has much more severe effects on archenteron elongation than does the blockage of convergent extension with Xdd1 reported here.

We suggest that convergent extension and epiboly drive distinct aspects of archenteron elongation. If this is the case, then molecular perturbations that disrupt both epiboly and convergent extension should have very severe effects on archenteron formation. This is in fact the case, as disruption of fibronectin function results in defects in both epiboly and convergent extension, and in these embryos no archenteron ever forms (Marsden and DeSimone, 2001; Marsden and DeSimone, 2003). Disruption of Wee1 signaling also disrupts convergent extension, and to a lesser degree epiboly, and again results in a severe failure of archenteron formation (Murakami et al., 2004). These very severe archenteron defects resulting from these molecular disruptions are likely to represent the sum of defects in multiple motors contributing to archenteron elongation.

To highlight the potential contribution of epiboly to archenteron formation, it is informative to compare *Xenopus* gastrulation with that in the sturgeon, where the cell behaviors driving distinct tissue movements are similar, but where the different tissue movements are used in different ways (Bolker, 1994). Sturgeon gastrulation begins with robust epiboly commensurate with archenteron elongation, only later does convergent extension begin in earnest (Bolker, 1993a; Bolker,

1993b), suggesting that epiboly can contribute to the formation of an archenteron in the absence of convergent extension.

In order to elongate the archenteron, the vegetal-ward movement of superficial tissue driven by epiboly would need to work in concert with animal-ward movement of internal tissue. So, another likely contributor to archenteron elongation is active movement of vegetal yolk cells by vegetal rotation (Winklbauer and Schurfeld, 1999). Active, animal-ward movements continue in the yolk cells until late gastrula stages (Ibrahim and Winklbauer, 2001), and could drive archenteron elongation. Alternatively, intercalation of archenteron cells around the circumference of the forming gut tube could produce convergent-extension movements of the archenteron epithelium and thereby elongate it. Such a mechanism elongates tubes in echinoderm archenterons and in *Drosophila* hindgut tubes (Ettensohn, 1999; Lengyel and Iwaki, 2002).

Archenteron inflation

Our data suggest that the inflation and the elongation of the archenteron are separable morphogenetic events (Figs 9, 13). The mechanisms specifically governing archenteron inflation remain obscure, but it is likely that bottle cell respreading contributes to both archenteron inflation and elongation (Keller, 1975; Keller, 1981). Moreover, our 3D datasets demonstrate that archenteron inflation could be driven by the transfer of fluid from the blastocoel to the archenteron (Fig. 12) (see also Adolph, 1967; Humphrey, 1960; Tuft, 1957; Tuft, 1965; Zotin, 1965).

It is interesting that embryos deficient in convergent extension of dorsal tissues form relatively normal-looking archenterons by the tailbud stages (Fig. 10). Beginning during neurulation, the archenteron will eject fluid and shrink (Brown, 1941; Zotin, 1965), and the entire archenteron will eventually disappear before the onset of formation of the definitive gut (Chalmers and Slack, 2000). It has been suggested that the archenteron is a crucial organ for both fluid balance and for respiration (Adolph, 1967; Brown, 1941), but it is also possible that the archenteron is in fact most important as a morphogenetic device.

There is much evidence to suggest that fluid transfer in embryos can contribute to morphogenesis (Desmond and Jacobson, 1977). For example, the blastocoel is necessary as a space into which the internalized material can move (Eakin, 1939), and the rapid transfer of fluid from blastocoel to archenteron may be a necessary consequence of this invasion of material. Indeed, dye experiments in sturgeon, *Xenopus* and *Ambystoma* have indicated that fluid is transferred from blastocoel to archenteron during gastrulation (Humphrey, 1960; Tuft, 1957; Zotin, 1965).

Defects in fluid transfer may explain some of the phenotypes observed in embryos lacking Xdsh function. Gastrulation movements, in particular the constriction of the blastopore, have been suggested to exert hydrostatic pressure on the blastocoel, forcing fluid into the archenteron (Zotin, 1965). So, by disrupting the progress of the blastopore lip, Xdd1 could indirectly reduce the pressure on the blastocoel. Indeed, we often observed a failure of blastocoel shrinkage in Xdd1-injected embryos (Fig. 4B, Fig. 11A). In turn, defects in the constriction of the blastopore would then also secondarily influence archenteron inflation, which may explain the different effects of Xdd1 injection on archenteron inflation and elongation (Figs 9, 11).

Evolutionary implications of the loose coupling of morphogenetic processes during gastrulation

There is tremendous variety in the overall sequences and patterns of morphogenetic processes during gastrulation in amphibians (Chipman et al., 1999; del Pino, 1996; Minsuk and Keller, 1996; Purcell and Keller, 1993; Shook et al., 2002; Shook et al., 2004). For example, although the marginal zone of salamander embryos undergoes convergent extension by mediolateral intercalation, this convergent extension does not drive blastopore closure; it is instead the subduction of surface mesoderm that forms arcs of hoop stress and drives blastopore closure in that species (Shi et al., 1987; Shook et al., 2002). Likewise embryos of *Gastrotheca* close their blastopores prior to the onset of convergent extension (del Pino, 1996). Moreover, gastrulation in the frog *Hyperolius puncticulatus* more closely resembles that of the sturgeon, with a near-completion of epiboly occurring prior to the onset of internalization at the blastopore, or of axis elongation (Bolker, 1993a; Chipman et al., 1999). In addition, the yolk-rich gastrulae of this frog species form very small blastocoels and also very small, slit-like archenterons (Chipman et al., 1999).

The *Xenopus* archenteron can elongate significantly during late gastrulation in the nearly complete absence of elongation of the axial mesoderm by convergent extension (Figs 9, 14), and the marginal zone and yolk plug material can be internalized in the absence of blastopore closure (Figs 4, 5). These findings suggest that each of the morphogenetic programs that run in parallel during gastrulation can act to a large degree independently of one another, yet can still function together as a whole.

Changes in gastrulation mechanisms could play an important role in the diversification of egg size and life history strategies in Amphibia (see Arendt and Nubler-Jung, 1999). As such, the observed dissociability of morphogenetic events during gastrulation may be evolutionarily significant. If the different aspects of frog gastrulation were more tightly coupled, then it would be relatively difficult to change one element without severe consequences on other processes. If this were the case, one would expect that relatively similar gastrulation processes would be observed in different amphibian species. Because the Amphibia display a wide diversity of patterns of gastrulation, we suggest that the lack of coupling between morphogenetic processes observed in *Xenopus* gastrulation reflects allowances for variability in the timing and the relative contributions of different events in gastrulation. This variability may in turn have allowed for evolutionary innovations that led to the diverse gastrulation patterns observed in amphibians.

We thank R. Harland, D. Parichy, D. Koos, C. Papan and S. Haigo for useful conversations and technical assistance. We thank Resolution Sciences Corporation (now Microscience Group) for instrument time; and R. Kerschmann, M. Reddington, L. Garrett, P. Guthrie, M. Bolles, M. Haugh and B. Herrera for technical assistance with SIM. A.J.E. thanks Z. Werb for space and support during the writing of this manuscript. This work was supported by funding from the Burroughs Wellcome Fund Interfaces Program via the Caltech Initiative in Computational Molecular Biology to A.J.E.; by an NIH R01 grant to Richard M. Harland; an NIH NICHD grant to S.E.F.; and by a Career

Award in the Biomedical Sciences from the Burroughs Wellcome Fund to J.B.W.

Supplementary material

Supplementary material for this article is available at
http://dev.biologists.org/cgi/content/full/131/24/6195/DC1

References

Abramoff, M. D., Niessen, W. J. and Viergever, M. A. (2000). Objective quantification of the motion of soft tissues in the orbit. *IEEE Trans. Med. Imaging* **19**, 986-995.

Adolph, E. F. (1967). Ontogeny of volume regulations in embryonic extracellular fluids. *Q. Rev. Biol.* **42**, 1-39.

Arendt, D. and Nubler-Jung, K. (1999). Rearranging gastrulation in the name of yolk: evolution of gastrulation in yolk-rich amniote eggs. *Mech. Dev.* **81**, 3-22.

Barron, J. L., Fleet, D. J. and Beauchemin, S. S. (1994). Performance of optical-flow techniques. *Int. J. Comp. Vis.* **12**, 43-77.

Beloussov, L. V., Dorfman, J. G. and Cherdantzev, V. G. (1975). Mechanical stresses and morphological patterns in amphibian embryos. *J. Embryol. Exp. Morphol.* **34**, 559-574.

Beloussov, L. V., Lakirev, A. V., Naumidi, I. I. and Novoselov, V. V. (1990). Effects of relaxation of mechanical tensions upon the early morphogenesis of Xenopus laevis embryos. *Int. J. Dev. Biol.* **34**, 409-419.

Beloussov, L. V., Louchinskaia, N. N. and Stein, A. A. (2000). Tension-dependent collective cell movements in the early gastrula ectoderm of Xenopus laevis embryos. *Dev. Genes Evol.* **210**, 92-104.

Bolker, J. A. (1993a). Gastrulation and mesoderm morphogenesis in the white sturgeon. *J. Exp. Zool.* **266**, 116-131.

Bolker, J. A. (1993b). The mechanism of gastrulation in the white sturgeon. *J. Exp. Zool.* **266**, 132-145.

Bolker, J. A. (1994). Comparison of gastrulation in frogs and fishes. *Am. Zool.* **34**, 313-322.

Brown, M. G. (1941). Collapse of the archenteron in embryos of Amblystoma and Rana. *J. Exp. Zool.* **88**, 95-106.

Chalmers, A. D. and Slack, J. M. (2000). The Xenopus tadpole gut: fate maps and morphogenetic movements. *Development* **127**, 381-392.

Chipman, A. D., Haas, A. and Khaner, O. (1999). Variations in anuran embryogenesis: yolk-rich embryos of Hyperolius puncticulatus (Hyperoliidae). *Evol. Dev.* **1**, 49-61.

Cooke, J. (1985). Dynamics of the control of body pattern in the development of Xenopus laevis. III. Timing and pattern after u.v. irradiation of the egg and after excision of presumptive head endo-mesoderm. *J. Embryol. Exp. Morphol.* **88**, 135-150.

Darken, R. S., Scola, A. M., Rakeman, A. S., Das, G., Mlodzik, M. and Wilson, P. A. (2002). The planar polarity gene strabismus regulates convergent extension movements in Xenopus. *EMBO J.* **21**, 976-985.

Davidson, L. A., Hoffstrom, B. G., Keller, R. and DeSimone, D. W. (2002). Mesendoderm extension and mantle closure in Xenopus laevis gastrulation: combined roles for integrin alpha(5)beta(1), fibronectin, and tissue geometry. *Dev. Biol.* **242**, 109-129.

Deardorff, M. A., Tan, C., Conrad, L. J. and Klein, P. S. (1998). Frizzled-8 is expressed in the Spemann organizer and plays a role in early morphogenesis. *Development* **125**, 2687-2700.

del Pino, E. M. (1996). The expression of Brachyury (T) during gastrulation in the marsupial frog Gastrotheca riobambae. *Dev. Biol.* **177**, 64-72.

Desmond, M. E. and Jacobson, A. G. (1977). Embryonic brain enlargement requires cerebrospinal fluid pressure. *Dev. Biol.* **57**, 188-198.

Eakin, R. (1939). Further studies on the regulatory development of Tritorus torosus. *Univ. Cal. Pub. Zool.* **43**, 185-209.

Ettensohn, C. A. (1999). Cell movements in the sea urchin embryo. *Curr. Opin. Genet. Dev.* **9**, 461-465.

Ewald, A. J., McBride, H., Reddington, M., Fraser, S. E. and Kerschmann, R. (2002). Surface imaging microscopy, an automated method for visualizing whole embryo samples in three dimensions at high resolution. *Dev. Dyn.* **225**, 369-375.

Gerhart, J., Danilchik, M., Doniach, T., Roberts, S., Rowning, B. and Stewart, R. (1989). Cortical rotation of the Xenopus egg: consequences for the anteroposterior pattern of embryonic dorsal development. *Development* **107**, 37-51.

Goto, T. and Keller, R. (2002). The planar cell polarity gene Strabismus regulates convergence and extension and neural fold closure in *Xenopus*. *Dev. Biol.* **247**, 165-181.

Gregg, J. R. (1957). Morphogenesis and metabolism of gastrulation-arrested embryos in the hybrid Rana Pipiens x Rana sylvatica. In *The Beginnings of Embryonic Development* (ed. A. Tyler, R. C. von Borstel and C. B. Metz), pp. 231-261. Washington, DC: Am. Assoc. Adv. Sci.

Gregg, J. R. and Klein, D. (1955). Morphogenetic movements of normal and gastrula-arrested hybrid amphibian tissues. *Biol. Bull.* **109**, 365-370.

Hasegawa, K. and Kinoshita, T. (2000). Xoom is required for epibolic movement of animal ectodermal cells in Xenopus laevis gastrulation. *Dev. Growth Differ.* **42**, 337-346.

Holtfreter, J. (1944). A study of the mechanics of gastrulation, Part II. *J. Exp. Zool.* **95**, 171-212.

Humphrey, R. R. (1960). A maternal effect gene (f) for fluid imbalance in the Mexican axolotl. *Dev. Biol.* **2**, 105-128.

Ibrahim, H. and Winklbauer, R. (2001). Mechanisms of mesendoderm internalization in the Xenopus gastrula: lessons from the ventral side. *Dev. Biol.* **240**, 108-122.

Keller, R. E. (1975). Vital dye mapping of the gastrula and neurula of Xenopus laevis. I. Prospective areas and morphogenetic movements of the superficial layer. *Dev. Biol.* **42**, 222-241.

Keller, R. E. (1981). An experimental analysis of the role of bottle cells and the deep marginal zone in gastrulation of Xenopus laevis. *J. Exp. Zool.* **216**, 81-101.

Keller, R. E. (1984). The cellular basis of gastrulation in Xenopus: active, postinvolution convergence and extension by mediolateral interdigitation. *Amer. Zool.* **24**, 589-603.

Keller, R. and Danilchik, M. (1988). Regional expression, pattern and timing of convergence and extension during gastrulation of Xenopus laevis. *Development* **103**, 193-209.

Keller, R. and Jansa, S. (1992). Xenopus Gastrulation without a blastocoel roof. *Dev. Dyn.* **195**, 162-176.

Keller, R. E., Danilchik, M., Gimlich, R. and Shih, J. (1985). The function and mechanism of convergent extension during gastrulation of Xenopus laevis. *J. Embryol. Exp. Morphol.* **89**, 185-209.

Keller, R., Davidson, L. A. and Shook, D. R. (2003). How we are shaped: the biomechanics of gastrulation. *Differentiation* **71**, 171-205.

Kominami, T. and Takata, H. (2000). Cellular basis of gastrulation in the sand dollar Scaphechinus mirabilis. *Biol. Bull.* **199**, 287-297.

Lengyel, J. A. and Iwaki, D. D. (2002). It takes guts: the Drosophila hindgut as a model system for organogenesis. *Dev. Biol.* **243**, 1-19.

Lucas, B. and Kanade, T. (1981). An Iterative Image Registration Technique with an Application to Stereo Vision. In *Proceedings of the DARPA Image Understanding Workshop*, pp. 121-130.

Malacinski, G. M., Brothers, A. J. and Chung, H. M. (1977). Destruction of components of the neural induction system of the amphibian egg with ultraviolet irradiation. *Dev. Biol.* **56**, 24-39.

Marsden, M. and DeSimone, D. W. (2001). Regulation of cell polarity, radial intercalation and epiboly in Xenopus: novel roles for integrin and fibronectin. *Development* **128**, 3635-3647.

Marsden, M. and DeSimone, D. W. (2003). Integrin-ECM interactions regulate cadherin-dependent cell adhesion and are required for convergent extension in Xenopus. *Curr. Biol.* **13**, 1182-1191.

Medina, A., Reintsch, W. and Steinbeisser, H. (2000). Xenopus frizzled 7 can act in canonical and non-canonical Wnt signaling pathways: implications on early patterning and morphogenesis. *Mech. Dev.* **92**, 227-237.

Minsuk, S. B. and Keller, R. E. (1996). Dorsal mesoderm has a dual origin and forms by a novel mechanism in Hymenochirus, a relative of Xenopus. *Dev. Biol.* **174**, 92-103.

Moon, R. T., Campbell, R. M., Christian, J. L., McGrew, L. L., Shih, J. and Fraser, S. (1993). Xwnt-5A: a maternal Wnt that affects morphogenetic movements after overexpression in embryos of Xenopus laevis. *Development* **119**, 97-111.

Moore, J. A. (1946). Studies in the development of frog hybrids. I. Embryonic development in the cross Rana pipiens × Rana sylvatica. *J. Exp. Zool.* **101**, 173-219.

Moore, S. W., Keller, R. E. and Koehl, M. A. (1995). The dorsal involuting marginal zone stiffens anisotropically during its convergent extension in the gastrula of Xenopus laevis. *Development* **121**, 3131-3140.

Murakami, M. S., Moody, S. A., Daar, I. O. and Morrison, D. K. (2004). Morphogenesis during Xenopus gastrulation requires Wee1-mediated inhibition of cell proliferation. *Development* **131**, 571-580.

Nagel, M., Tahinci, E., Symes, K. and Winklbauer, R. (2004). Guidance of

mesoderm cell migration in the Xenopus gastrula requires PDGF signaling. *Development* **131**, 2727-2736.

Nakatsuji, N. (1974). Studies on the gastrulation of amphibian embryos, numerical criteria for stage determination during blastulation and gastrulation of Xenopus leavis. *Dev. Growth Differ.* **16**, 257-265.

Nieuwkoop, P. D. and Faber, J. (1994). *Normal Table of Xenopus laevis (Daudin)*. New York, NY: Garland.

Park, M. and Moon, R. T. (2002). The planar cell-polarity gene stbm regulates cell behaviour and cell fate in vertebrate embryos. *Nat. Cell Biol.* **4**, 20-25.

Phillips, H. M. (1984). Physical analysis of tissue mechanics in amphibian gastrulation. *Am. Zool.* **24**, 657-672.

Purcell, S. M. and Keller, R. (1993). A different type of amphibian mesoderm morphogenesis in Ceratophrys ornata. *Development* **117**, 307-317.

Reintsch, W. E. and Hausen, P. (2001). Dorsoventral differences in cell-cell interactions modulate the motile behaviour of cells from the Xenopus gastrula. *Dev. Biol.* **240**, 387-403.

Rothbächer, U., Laurent, M. N., Deardorff, M. A., Klein, P. S., Cho, K. W. Y. and Fraser, S. E. (2000). Dishevelled phosphorylation, subcellular localization and homomerization regulate its role in early embryogenesis. *EMBO J.* **19**, 1010-1022.

Schectman, A. M. (1942). The mechanics of amphibian gastrulation. *Univ. Calif. Pub. Zool.* **51**, 1-39.

Shi, D. L., Delarue, M., Darribere, T., Riou, J. F. and Boucaut, J. C. (1987). Experimental analysis of the extension of the dorsal marginal zone in Pleurodeles waltl gastrulae. *Development* **100**, 147-161.

Shih, J. and Keller, R. (1992a). Cell motility driving mediolateral intercalation in explants of Xenopus laevis. *Development* **116**, 901-914.

Shih, J. and Keller, R. (1992b). Patterns of cell motility in the organizer and dorsal mesoderm of Xenopus laevis. *Development* **116**, 915-930.

Shih, J. and Keller, R. (1994). Gastrulation in Xenopus: involution – a current view. *Semin. Dev. Biol.* **5**, 85-90.

Shook, D. R., Majer, C. and Keller, R. (2002). Urodeles remove mesoderm from the superficial layer by subduction through a bilateral primitive streak. *Dev. Biol.* **248**, 220-239.

Shook, D. R., Majer, C. and Keller, R. (2004). Pattern and morphogenesis of presumptive superficial mesoderm in two closely related species, Xenopus laevis and Xenopus tropicalis. *Dev. Biol.* **270**, 163-185.

Sive, H. L., Grainger, R. M. and Harland, R. M. (2000). *Early Development of Xenopus laevis: A Laboratory Manual*. Cold Spring Harbor, NY: Cold Spring Harbor Press.

Sokol, S. Y. (1996). Analysis of Dishevelled signalling pathways during Xenopus development. *Curr. Biol.* **6**, 1456-1467.

Takeuchi, M., Nakabayashi, J., Sakaguchi, T., Yamamoto, T. S., Takahashi, H., Takeda, H. and Ueno, N. (2003). The Prickle-related gene in vertebrates is essential for gastrulation cell movements. *Curr. Biol.* **13**, 674-679.

Tuft, P. (1957). The osmotic activity of the blastocoel and archenteron fluids. *Proc. R. Physiol. Soc. Edinb.* **26**, 42-48.

Tuft, P. (1965). The uptake and distribution of water in the developing amphibian embryo. *Symp. Soc. Exp. Biol.* **19**, 385-403.

von Dassow, G., Schmidt, J. E. and Kimelman, D. (1993). Induction of the Xenopus organizer: expression and regulation of Xnot, a novel FGF and activin-regulated homeo box gene. *Genes Dev.* **7**, 355-366.

Wallingford, J. B., Sater, A. K., Uzman, J. A. and Danilchik, M. V. (1997). Inhibition of morphogenetic movement during Xenopus gastrulation by injected sulfatase: implications for anteroposterior and dorsoventral axis formation. *Dev. Biol.* **187**, 224-235.

Wallingford, J. B., Rowning, B. A., Vogeli, K. M., Rothbächer, U., Fraser, S. E. and Harland, R. M. (2000). Dishevelled controls cell polarity during *Xenopus* gastrulation. *Nature* **405**, 81-85.

Wallingford, J. B., Fraser, S. E. and Harland, R. M. (2002). Convergent extension: the molecular control of polarized cell movement during embryonic development. *Dev. Cell* **2**, 695-706.

Wilson, P. and Keller, R. (1991). Cell rearrangement during gastrulation of Xenopus: direct observation of cultured explants. *Development* **112**, 289-300.

Winklbauer, R. and Schurfeld, M. (1999). Vegetal rotation, a new gastrulation movement involved in the internalization of the mesoderm and endoderm in Xenopus. *Development* **126**, 3703-3713.

Winklbauer, R., Selchow, A., Nagel, M. and Angres, B. (1992). Cell interaction and its role in mesoderm cell migration during Xenopus gastrulation. *Dev. Dyn.* **195**, 290-302.

Zotin, A. I. (1965). The uptake and movement of water in the embryo. *Symp. Soc. Exp. Biol.* **19**, 365-384.